Macromolecules
ARTICLE

Macromolecules **2010**, *43*, 8239–8250 **8239**
DOI: 10.1021/ma101211b

Understanding Dynamics in Binary Mixtures of Entangled *cis*-1,4-Polybutadiene Melts at the Level of Primitive Path Segments by Mapping Atomistic Simulation Data onto the Tube Model

Chunggi Baig,[†] Pavlos S. Stephanou,[†] Georgia Tsolou,[†] Vlasis G. Mavrantzas,*[,†] and Martin Kröger[‡]

[†]*Department of Chemical Engineering, University of Patras & FORTH-ICE/HT, Patras GR 26504, Greece, and* [‡]*Polymer Physics, ETH Zürich, Department of Materials, Wolfgang-Pauli-Str. 10, CH-8093 Zürich, Switzerland*

Received May 31, 2010; Revised Manuscript Received August 16, 2010

ABSTRACT: We study dynamics in bidisperse melts of linear *cis*-1,4-polybutadiene composed of probe and matrix chains at the level of the segment survival probability function $\psi(s,t)$ which is computed directly in the course of long atomistic molecular dynamics simulations [Stephanou et al. *J. Chem. Phys.* **2010**, *132*, 124904]. By controlling precisely the matrix chain length and composition, the effect of contour length fluctuations (CLFs) and constraint release (CR) on melt dynamics is quantified. Our study shows that (a) the values of the static topological properties of the probe chains (e.g., the average value of their primitive path (PP) contour length and its fluctuation) remain unaltered in the different matrices, but (b) their dynamical properties (including $\psi(s,t)$ and its average over all segments s, $\Psi(t)$, the time autocorrelation function of the PP contour length, and the time autocorrelation function of the chain end-to-end vector) vary significantly from matrix to matrix. As the length of the matrix chains decreases, the functions $\psi(s,t)$ and $\Psi(t)$ describing the reptation relaxation of the probe chains are found to decrease more rapidly. Furthermore, the relaxation of longer probe chains is seen to be delayed as the concentration of shorter matrix chains decreases. Overall, our direct computational study proves that CR is the dominant relaxation mechanism in melts of long and short *cis*-1,4-polybutadiene chains accounting for the majority of differences observed in their relaxation dynamics in different environments (since CLFs appear to be unaffected by compositional differences); as a result, it has a profound effect on the linear viscoelastic properties of the melt, such as the spectra of storage and loss moduli. By further analyzing the mean-square displacement of atomistic segments in the different matrices, we find that while the tube diameter is constant in the mixtures with $M_S \geq M_e$ where M_S is the molecular weight of short chains and M_e the entanglement molecular weight, it gradually increases in the mixtures with $M_S < M_e$. How the simulation results compare with laboratory measurements on melts of bidisperse polymers reported in the literature is also discussed.

1. Introduction

Dynamics in entangled polymer melts and concentrated solutions is governed by topological interactions that prevent chain crossability.[1−3] To fully account for the topological interaction in these systems is practically impossible, given the enormous number of internal degrees of freedom needed to specify their configuration. Thus, to be able to obtain some useful information about their rheological properties, one should resort to a simplified description where the emphasis is placed rather on the large-scale motions of the polymer chains as a whole than on the more rapid wiggly motions of portions of the chain. The latter are known to make a negligible contribution to the steady-state flow properties. This simplification is due to Edwards,[4] who considered that in a concentrated polymer solution or melt the principal motion of the chain will be in the direction of its main backbone and not perpendicular to that because the topological constraints from the surrounding molecules will restrict its motion sideways. Building on this consideration, Edwards chose insightfully to describe the entire set of topological constraints on a polymer molecule by introducing the concept of the effective curvilinear *tube*: it defines the space through which the chain can move in order to avoid the constraints imposed by "other" chains. Later, Edwards introduced also the notion of the primitive path (PP) referring to a coarse-grained representation of the polymer chain; the concept turned out to be particularly useful in the statistical description of chain conformations in the presence of topological constraints.[5] An analytical solution to the problem of chain dynamics in the presence of topological constraints was given by de Gennes,[6] who considered the motion of an isolated chain in a fixed network of obstacles. Here, the diameter of the effective curvilinear tube is approximately equal to the average mesh spacing of the network, and the only possible motion that the chain can execute at length scales larger than the tube diameter is considered to be reptation (curvilinear diffusion) along the tube. Building on the concepts of "tube constraints" and "reptation", Doi and Edwards[7] developed the well-known reptation or tube theory (perhaps the most comprehensive theory so far) for the dynamics of polymers in entangled melts and concentrated solutions, which revealed how distinctly different their rheological behavior is in comparison to unentangled ones.

Despite its success, the original Doi−Edwards model[3,7] was not fully consistent with some important experimental observations. For example, the model predicts that the zero-shear viscosity of an entangled polymer melt should scale with the molecular weight

*To whom correspondence should be addressed: e-mail vlasis@chemeng.upatras.gr, Tel +30-2610-997398, Fax +30-2610-965223.

Published on Web 09/09/2010

M as $\eta_0 \sim M^3$ whereas the experimental measurements[1−3] are in support of a scaling law of the form $\eta_0 \sim M^{3.4}$. The degree of shear thinning is overestimated, and the prediction that $D_G \sim M^{-2}$ for the chain center-of-mass self-diffusion coefficient (D_G) does not agree with experimental data according to which $D_G \sim M^{-2.2}$.[3,7] These discrepancies, among others, led investigators in the field to propose and explore additional relaxational mechanisms for entangled systems besides chain reptation. Two of them are known today as contour length fluctuation (CLF)[8] and constraint release (CR).[9−11] CLF accounts for the dynamical variation of the PP contour length of the chain with time and CR for the dynamical variation of the topological constraints or the effective tube with time. CLF is basically considered as a single-chain mechanism which renders its incorporation into the theory generally straightforward (although an exact quantitative description is still missing). Incorporating (analytically) the CR effect, on the other hand, into the theory is a much more difficult and challenging task because it essentially involves the dynamics of all the surrounding chains. Numerous theoretical works have appeared so far accounting for the CR effect in the one or the other way.[9−19] Although these have led to significant improvements as far as comparison with experimental data is concerned, a fundamental understanding of the CR mechanism and its exact mathematical treatment are still lacking.

Topological constraints are intimately connected with the motion of surrounding chains. As such, the role of the CR mechanism is expected to be particularly important in polydisperse systems (consisting of polymer molecules with different chain lengths) due to the different lifetimes of entanglements corresponding to the different chain length species present in the system. A prototypical, while particularly simple, system for assessing CR effects is thus that of a bidisperse polymer melt, i.e., a binary mixture composed of two chemically identical polymer species which differ only in their molecular weight. Such mixtures have been used quite extensively in the literature to study the diffusion behavior[20−26] of long and short polymer chains and their related viscoelastic properties.[22,26−31] For example, today it is rather well accepted that a long chain in a short-chain matrix diffuses faster as the matrix chain length decreases or the concentration of the long chain decreases. Concerning viscoelastic properties, on the other hand, Struglinski and Graessley[29] carried out a systematic experimental study of CR using well-defined binary mixtures of linear polybutadienes with variable chain length and composition. It was found that keeping the chain lengths of the two components constant, rheological properties (such as the zero-shear viscosity η_0, the steady-state shear compliance J_e^0, and the storage $G'(\omega)$ and loss $G''(\omega)$ moduli) depend strongly on the volume fraction ϕ_L of the long component.[29] Struglinski and Graessley[29] observed also a decrease in the peak frequency $(\omega_{max})_S$ of $G''(\omega)$ that corresponds to the short-chain species with increasing ϕ_L, although there appeared nearly no variation in the peak frequency $(\omega_{max})_L$ of the longer species. The apparent constant value of $(\omega_{max})_L$ was attributed to the relatively small values of the Struglinski−Graessley ratio $r_{SG} \equiv M_L M_e^2/M_S^3$ (M_L denotes the molecular weight of the long chains, M_S the molecular weight of the short chains, and M_e the entanglement molecular weight) for the binary mixtures studied in their work. It was reported that the crossover value of r_{SG} for the dependence of $(\omega_{max})_L$ on ϕ_L is approximately equal to 0.1.[29]

On the basis of these interesting experimental results,[22,28,29] Doi et al.[32] provided a detailed theoretical account of CR by introducing the concept of tube dilation (the increase in the effective tube diameter) based on the relative displacements of the reptating chain and the Rouse-like tube where the tube constraints are made by both short and long chains. More specifically, if a chain moves slower than the tube, the chain is assumed not to feel any tube constraints; only when the chain motion is faster than that of the tube is the tube supposed to effectively constrain the chain dynamics. The effective tube diameter is then taken to be equal to the displacement where the chain and the tube motions cross each other. Although only qualitative (due to the very approximate treatment of the effective tube diameter), the Doi et al.[32] theory appeared to explain general experimental observations conceptually well; it further provided a systematic analysis of how much and under what conditions (M_L, M_S, ϕ_L) a binary mixture will exhibit different rheological behaviors (with respect, e.g., to the relaxation time of the long chains and the relaxation modulus).[32]

Doi et al.'s theory for taking into account CR was further elaborated by Viovy et al.,[33] who hypothesized that tube dilation can occur if there exist topological constraints imposed by chains whose molecular length is smaller than the average entanglement length of the system. Furthermore, they assumed that the Rouse motion of the tube is possible only up to a value that is equal to the length between entanglements made by the long chains, $a_L = a/\sqrt{\phi_L}$ where a is the original tube diameter; beyond that length scale, they assumed a new process called *tube reptation* to get activated, instead of the tube dilation as conjectured by Doi et al.[32] Although the specific concepts are different in the two approaches, they bear many similarities in their predictions for the relaxation behavior of binary systems. At the same time, we should keep in mind the important distinction between the two theories: while Doi et al.[32] assumed that tube dilation can occur whenever the overall chain motion is slower than the tube motion, Viovy et al.[33] considered it to be possible only when $M_S < M_e$. From a physical point of view, it seems that chain segments would always start to feel the topological constraints imposed by surrounding chains at the same length scale corresponding to M_e, independent of the molecular weight of surrounding chains as long as this is above M_e. Very interestingly, as we will discuss below, the present analysis of the atomistic segmental mean-square displacement (msd) in the various bidisperse polymer melts shows that while the tube diameter is constant for the binary mixtures with $M_S \geq M_e$, it appears to increase in the mixtures with $M_S < M_e$, thus supporting Viovy et al.'s proposition.

A fundamental understanding of CR requires detailed information about chain dynamics at molecular length and time scales, a piece which unfortunately is very difficult to obtain from laboratory experiments. Such information is, however, obtainable by molecular simulations. In fact, there have appeared a few simulation works in the literature employing Monte Carlo[34,35] or coarse-grained molecular dynamics (MD) simulation methods[36,37] to study the diffusional behavior of polymer chains in bidisperse mixtures with different matrix chain lengths and compositions. The general trends revealed in those works were seen to be consistent with experimental observations. However, due to the use of a coarse-grained model, direct quantitative analysis and comparison against experimental data were impossible.

In this work we study in detail how the matrix environment in bidisperse mixtures affects their rheological properties. To this, we have carried out extensive atomistic MD simulations with a variety of bidisperse linear polybutadiene (PB) melts of moderate chain lengths,[38] whose dynamics should be dominated by strong CR effects. By applying a recently developed computational methodology,[39] we have been able to extract the dynamics of primitive chain segments by mapping the atomistic MD trajectories onto trajectories of PPs. This has allowed us to obtain the segment survival probability function $\psi(s,t)$ and the overall tube survival probability $\Psi(t)$ separately for the long and short chains in the mixture. In fact, as explained in detail in the original paper,[39] the results of such an approach for $\psi(s,t)$ and $\Psi(t)$ include all possible dynamical effects by the CLF and CR

mechanisms (and others) on chain relaxation, since they are automatically captured in the atomistic simulations and thus are directly reflected in the primitive chain trajectory via the geometric mapping from the finer (atomistic) level to the coarser (PP) one. We refer the interested reader to the original paper[39] for methodological details. On the basis of the results thus obtained, here we provide a detailed quantitative analysis on the individual aspects of CLF and CR on the relaxation behavior of bidisperse polymers.

The paper is organized as follows: In section 2, we discuss briefly the simulation method and details of the molecular systems addressed in our study. In section 3 we present detailed results for the functions $\psi(s,t)$ and $\Psi(t)$ for the short and long components in the simulated binary mixtures and the role of CR and CLF on their relaxation. We also recast the results in terms of the frequency spectra of storage and loss moduli. In section 4 we summarize the most important conclusions of the present work and propose future research directions.

2. Simulation Method and Systems Studied

A classical united-atom model has been adopted in all of our simulations with the *cis*-1,4-PB systems, according to which methyl (CH_3), internal methylene (CH_2), and methyne (CH) units are treated as single interacting sites. The specific form of the potential functions describing bonded and nonbonded interactions in the system have been borrowed from the work of Gee and Boyd[40] and Smith and Paul.[41] To avoid unnecessary repetitions, readers interested in the details of the force field and its parametrization are referred to a previous paper.[42]

The MD simulations have been carried out at temperature T = 413 K and pressure P = 1 atm using the LAMMPS (large-scale atomic/molecular massively parallel simulator) code.[43] The set of equations of motion corresponding to the *NPT* statistical ensemble (N denotes the total number of atomistic units in the simulation cell) was numerically integrated using the reversible Reference System Propagator Algorithm (r-RESPA)[44] with two different time scales for each MD step: a large equal to 2 fs and a small equal to 1 fs. Sufficiently long atomistic trajectories were accumulated for each system in order to reduce the statistical uncertainty and increase the numerical accuracy of the computed average values.

All model binary mixtures considered here are *cis*-1,4-PB melts composed of two types of chains: probe and matrix. The probe chains were always C_{600} *cis*-1,4-PB molecules whose molecular weight corresponds approximately to $4.2M_e$ ($M_e \approx 1946$ g/mol amounting to a C_{144} *cis*-1,4-PB chain).[39] For the matrix chains, four different chain lengths were considered corresponding to C_{100} ($\sim 0.7M_e$), C_{200} ($\sim 1.4M_e$), C_{320} ($\sim 2.2M_e$), and C_{1000} ($\sim 6.9M_e$) *cis*-1,4-PB molecules. For each binary mixture, two or three different volume fractions ϕ_p of the probe chains were studied in order to investigate the effect of their concentration (matrix composition) on the dynamic properties of the system. Note also that $\phi_p = \phi_L$ for all systems in this study except the C_{1000}-C_{600} mixtures for which $\phi_p = 1 - \phi_L$. The PP network for each of the simulated systems was extracted by making use of the so-called Z1-code,[45] which returns the shortest multiple disconnected path for a given atomistic configuration. The tube diameter a around each probe chain was determined by analyzing the msd, $\phi(t) = \langle(\mathbf{r}_n(t) - \mathbf{r}_n(0))^2\rangle$, of its atomistic units in time, where $\mathbf{r}_n$ denotes the position vector of the nth atom along the chain (only the innermost atoms are included in the calculations to avoid chain-end effects). It was estimated as $a = 2[\phi(t^*)]^{1/2}$, where $\phi(t^*)$ is registered at time $t = t^*$ where the slope of $\phi(t)$ starts to change from the initial or $t^{1/2}$ regime (in a log−log plot) to the next or $t^{1/4}$ regime due to the onset of tube constraints on chain dynamics.[39] The corresponding $\psi(s,t)$ function is then computed by analyzing the time evolution of primitive chain segments in and out the effective tube enclosing the chain. Details are given in the original paper, ref 39.

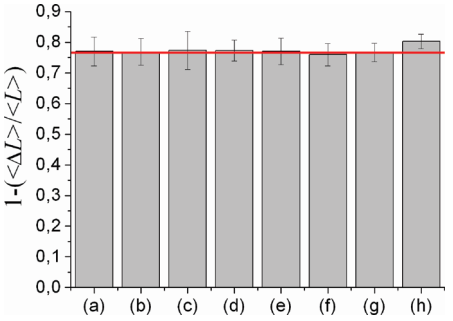

Figure 1. Average fluctuation of the PP contour length in different binary mixtures. Simulation results for the following systems: (a) *cis*100-*cis*600 (ϕ_p = 0.375), (b) *cis*100-*cis*600 (ϕ_p = 0.545), (c) *cis*200-*cis*600 (ϕ_p = 0.158), (d) *cis*200-*cis*600 (ϕ_p = 0.429), (e) *cis*320-*cis*600 (ϕ_p = 0.238), (f) *cis*320-*cis*600 (ϕ_p = 0.385), (g) *cis*320-*cis*600 (ϕ_p = 0.789), and (h) *cis*1000-*cis*600 (ϕ_p = 0.130). The horizontal red line represents the result for the pure component PB-*cis*600 melt.

3. Results and Discussion

In Figure 1 we look into matrix effects on the fluctuation $1 - \langle\Delta L\rangle/\langle L\rangle$ with $\langle\Delta L\rangle \equiv (\langle L^2\rangle - \langle L\rangle^2)^{1/2}$ of the PP contour length L of the probe (C_{600} *cis*-1,4-PB) chains. We see that the percentage of the fluctuation relative to $\langle L\rangle$ amounts approximately to 20−25% for all systems, including the pure component PB-*cis*600 melt. This shows that CLFs are not essentially influenced by the exact matrix chain length and composition, which is consistent with the view that CLF is a single-chain mechanism (thus, practically independent of the size or fraction of surrounding chains). We should regard therefore constraint release (CR) as the principal source for the variations observed in the rheological behavior of the probe chains in the different binary mixtures simulated in this work. To further elucidate the effect of matrix environment on the underlying topological network of the simulated melts, in Figure 2 we report the variation of the probability distribution function of (a) the number Z of entanglement strands per C_{600} probe chain and (b) the PP contour length L of C_{600} probe chain in the different systems. We observe (see Figure 2a) that not only the average value of Z but also its overall distribution is practically independent of matrix chain length and composition (at least for the systems studied here). By contrast, Masubuchi et al.[46] have reported a slight widening of $P(Z)$ for long chains as their volume fraction decreases. Such a discrepancy (which is not well understood at present) might be due to the coarse-grained nature of the slip-link simulations and/or to the moderate values of chain lengths addressed here. Figure 2b presents results for the distribution function $P(L)$ of the PP contour length L of the C_{600} probe chains. Similar to $P(Z)$, $P(L)$ is seen to be independent of the matrix environment within the statistical uncertainty of the numerical data. The general conclusion drawn from the results presented in Figures 1 and 2 is that the underlying topological structure of the simulated systems is not strongly influenced by variations in the matrix environment. With this in mind, we turn our attention next to the study of the dynamical properties of the simulated samples.

In Figure 3 we provide typical plots of the *instantaneous* values attained by the function $\psi(s,t)$ for s = 0.5 (the middle segment) for a randomly selected PB-*cis*600 probe chain in different polymer matrices. The value of $\psi(s,t)$ at short times is practically 1, then alternates between 1 and 0 as the segment fluctuates rapidly in and out the original tube, and finally drops to zero as the segment eventually escapes the tube. The time, however,

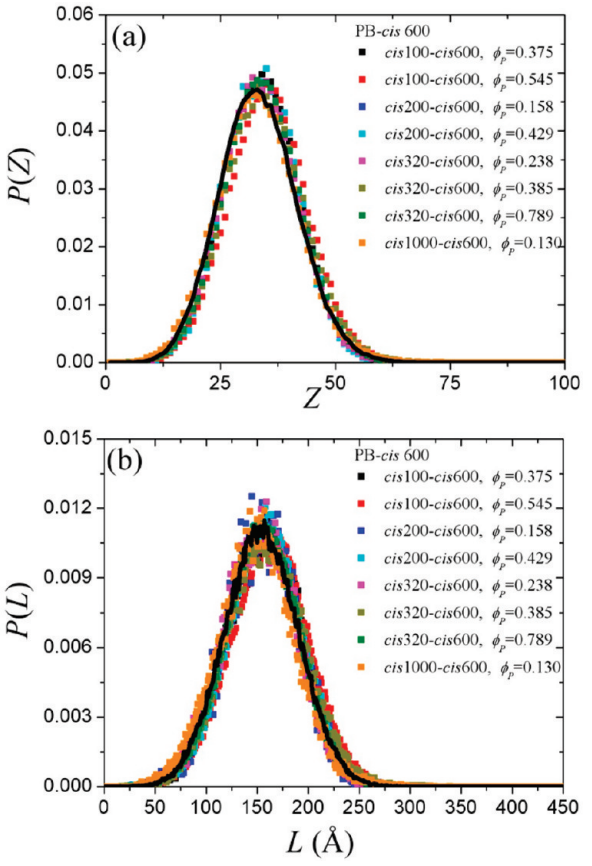

Figure 2. Probability distribution function of (a) the number Z of entanglement strands per C_{600} probe chain and (b) the PP contour length L of C_{600} probe chains in the simulated bidisperse melts. The corresponding results for the pure component PB-*cis*600 melt are shown by the thick black lines.

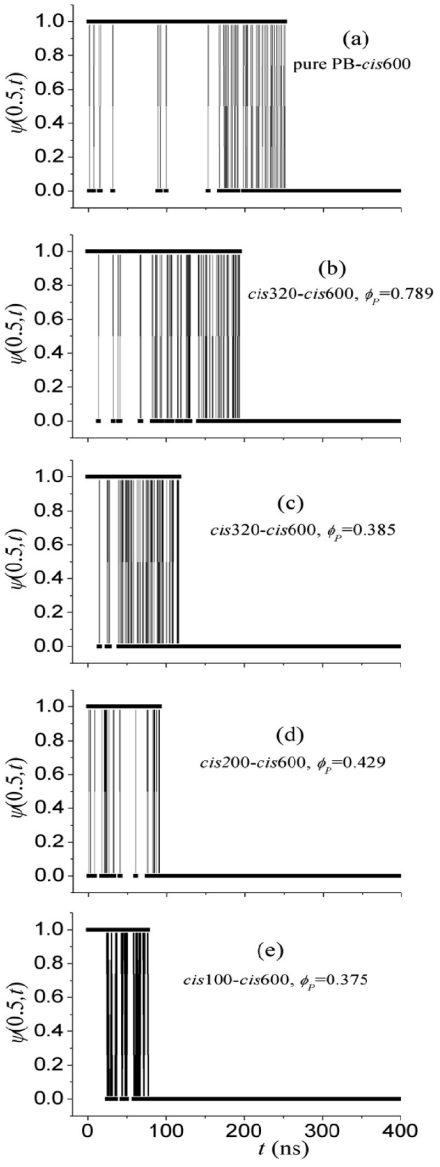

Figure 3. Typical plots of the instantaneous values attained by the function $\psi(s,t)$ for $s = 0.5$ (the middle segment) in different matrices. Simulation results for a randomly selected C_{600} *cis*-1,4-PB probe chain in the following melts: (a) pure component PB-*cis*600, (b) *cis*320-*cis*600 ($\phi_p = 0.789$), (c) *cis*320-*cis*600 ($\phi_p = 0.385$), (d) *cis*200-*cis*600 ($\phi_p = 0.429$), and (e) *cis*100-*cis*600 ($\phi_p = 0.375$).

it takes the segment to completely escape is different in the different matrices: for example, it is approximately equal to 250 ns in the pure component C_{600} matrix, equal to 200 ns in the C_{320} matrix with a volume fraction $\phi_p = 0.789$ in probe chains, equal to 120 ns in the C_{320} matrix with $\phi_p = 0.385$, and equal to 90 ns in the C_{200} matrix with $\phi_p = 0.429$. The numbers indicate significant differences which, given that fluctuations in the contour length of the probe chains have been computed above to be practically matrix independent, can only be explained if the CR effect is different in the different matrices. The value of $\psi(s = 0.5,t)$ averaged over all probe chains provides also a good estimate of the reptation (disentanglement) time of the probe chains.

Figure 4 presents results for the segment survival probability function $\psi(s,t)$ of the C_{600} *cis*-PB probe chains in the simulated binary mixtures, which are characterized by a similar concentration in probe chains but a different matrix chain length. Results are plotted as a function of segment position s in the normalized interval from 0 to 1, along the primitive chain ($s = 0$ and $s = 1$ representing the two chain ends and $s = 0.5$ the middle segment), at five time instances: (a) $t = 2$ ns, (b) $t = 7.5$ ns, (c) $t = 32$ ns, (d) $t = 106$ ns, and (e) $t = 211$ ns. These correspond to $\sim 1\tau_e$, $\sim 3\tau_e$, $\sim \tau_R/3$, $\sim \tau_R$, and $\sim \tau_d/2$, respectively, based on predicted MD values for the entanglement time $\tau_e = 2.3 \pm 0.8$ ns, the disentanglement time $\tau_d = 500 \pm 70$ ns, and the Rouse time $\tau_R = 90 \pm 15$ ns for PB-*cis*600 chains in their own melt at $T = 413$ K and $P = 1$ atm. They have been obtained by analyzing the MD data for the mean-square displacement of atomistic units on the basis of the reptation theory[3,39] (for τ_e and τ_d) and by making use of the scaling that $\tau_R \sim N^2$, knowing the τ_R times for a number of shorter unentangled *cis*-1,4-PB melts.[42] At the very early time (see Figure 4a), we see that the $\psi(s,t)$ curves for all binary mixtures are practically the same and very close to that of the pure component PB-*cis*600 melt, indicating that initially the C_{600} probe chains cannot distinguish *dynamically* between the different matrices as long as these are well entangled (composed of chains longer than C_{100} *cis*-1,4-PB). CR effects therefore associated with the relaxation dynamics of matrix chains are negligible at short times of the order of τ_e. We can analyze this issue further by considering that the entanglement length for *cis*-1,4-PB corresponds to a melt with chain length approximately equal to C_{144}.[39] The C_{100} *cis*-1,4-PB chain is thus below M_e, but on recalling that the molecular weight between true physical entanglements is in general half the value of M_e,[45,47,48] we can argue that even the C_{100} *cis*-1,4-PB chains supply topological constraints on the probe chains at short times. At a later time $t = 7.5$ ns, the computed $\psi(s,t)$ curves exhibit systematic deviations in the different systems (see Figure 4b): in the short-chain matrices (e.g., the *cis*100-*cis*600, *cis*200-*cis*600, and *cis*320-*cis*600 systems),

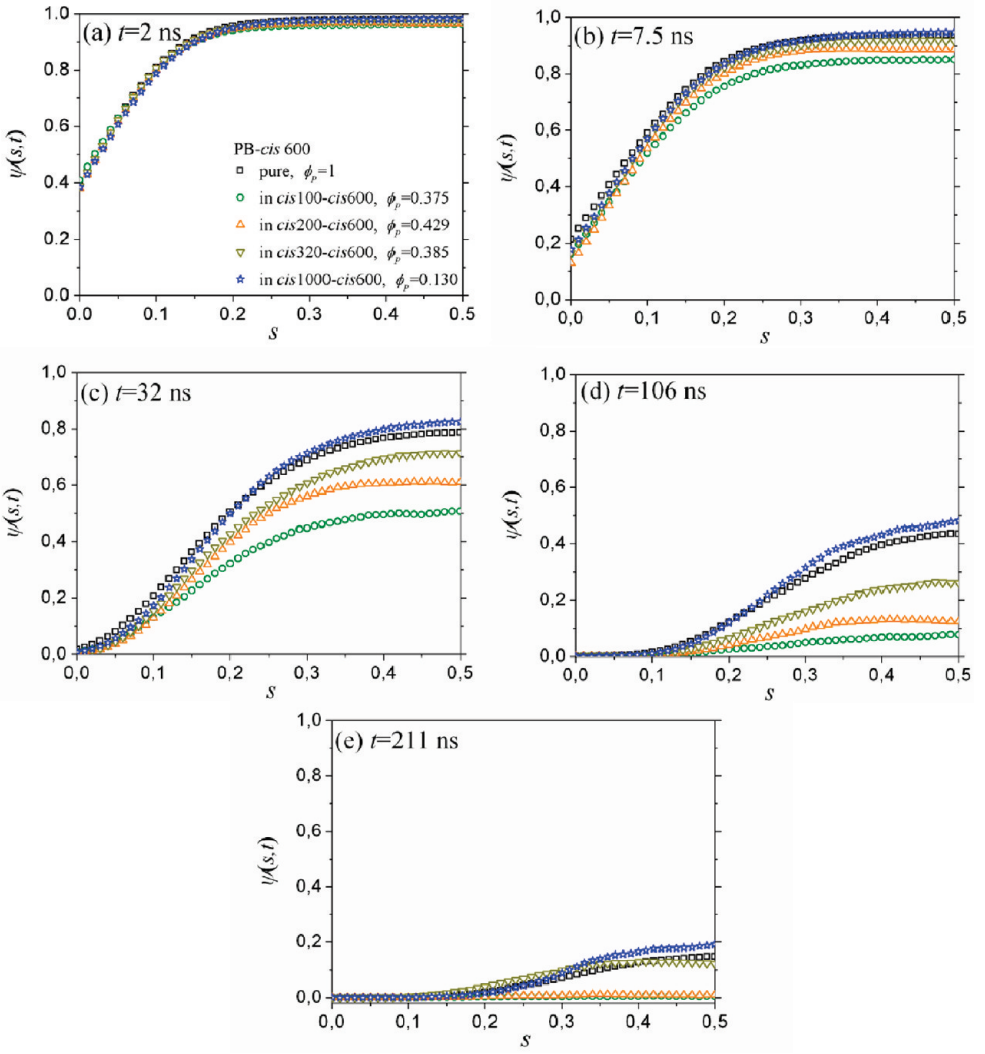

Figure 4. Segment survival probability function $\psi(s,t)$ for C_{600} *cis*-1,4-PB probe chains in different matrices and dependence on matrix chain length. Graphs of computed $\psi(s,t)$ profiles at (a) $t = 2$ ns ($\sim\tau_e$), (b) $t = 7.5$ ns ($\sim 3\tau_e$), (c) $t = 32$ ns ($\sim\tau_R/3$), (d) $t = 106$ ns ($\sim\tau_R$), and (e) $t = 211$ ns ($\sim\tau_d/2$). τ_e, τ_d, and τ_R here denote the characteristic entanglement, disentanglement, and Rouse times, respectively, of the C_{600} *cis*-1,4-PB chains in their own melt at $T = 413$ K and $P = 1$ atm. Their numerical values are[39,42,55] $\tau_e = 2.3 \pm 0.8$ ns, $\tau_d = 500 \pm 70$ ns, and $\tau_R = 90 \pm 15$ ns.

probe C_{600} *cis*-1,4-PB chains exhibit a faster relaxation than in their pure component PB-*cis*600 melt; in a long-chain matrix (e.g., the *cis*1000-*cis*600 system), on the other hand, they relax in time practically with the same rate as in their own melt. Furthermore, we see that probe chains relax faster as the matrix chain length decreases, a direct manifestation of CR effects associated with the relaxation of the short matrix chains at this time scale; this is particularly noticeable in the *cis*100-*cis*600 system. At even longer times, the computed $\psi(s,t)$ curves in the various binary mixtures are observed to depart even more (see, e.g., Figure 4c,d), confirming again the significant role of CR on chain relaxation. We also notice in Figure 4 that C_{600} chains in the *cis*1000-*cis*600 system relax slightly slower than in their own melt. This leads us to conclude that CR effects occur even in the strictly monodisperse C_{600} *cis*-1,4-PB melt due to the relaxation of neighboring chains around a tagged chain of exactly the same chain length. At the latest time, $t = 211$ ns, for which $\psi(s,t)$ curves are shown (see Figure 4e), the values of $\psi(s,t)$ for the *cis*100-*cis*600 and *cis*200-*cis*600 systems have fallen to zero for almost all primitive chain segments, pointing out to a complete relaxation of probe chains or, equivalently, to a complete renewal of the original tube.

A particularly noticeable feature in the plots of Figure 4 is that differences in the $\psi(s,t)$ values between the pure component and all binary systems are always smaller for segments s closer to the two chain ends. This reveals that the relative contribution of CLF and CR effects to the relaxation of primitive chain segments depends on how deeply the segment is embedded inside the chain contour. More precisely, segments near the ends of the chain relax rather quickly mainly via CLF and not via CR effects; the latter become active only at significantly longer times since they depend on the relaxation of the "other" chains. In sharp contrast, segments away from the two ends are affected less by CLFs (the corresponding effective time scales increasing exponentially with distance along the chain contour[3,19,49−51]); thus, their relaxation is mostly affected by CR. Such a result is further corroborated by the observation that the numerical data in Figure 4 for the function $\psi(s,t)$ are the same for segments $s \leq 0.1$ for almost all systems. This parallels closely the observations made in Figure 1 that only a part of the chain approximately equal to 20% its contour near the two ends is affected by CLFs. All these aspects brought up by our computational methodology should be useful in the analysis of experimental rheological data, since they indicate a need to consider different relaxation rates for different segments along the chain in theoretical models. For example, the additional feature that the function $\psi(s,t)$ attains a nonzero value at the two end segments ($s = 0$ and $s = 1$) for some finite time[39,52,53] has been explored by van Ruymbeke et al.[54] to resolve a systematic discrepancy in the predictions of tube models

with measured data for the plateau modulus of weakly entangled linear polymers. The effect of alignment of chain ends and the corresponding relaxation times on viscoelastic properties of polymer melts have also been discussed in ref 52. For reasons of completion, however, we provide in Figure 5 the corresponding results for the variation of $\psi(s = 0,t)$ and $\langle \mathbf{u}(s = 0,t)\cdot\mathbf{u}(s = 0,t = 0)\rangle$ with time t from the present study, for the simulated C_{600} probe chains in the various bidisperse systems. It is evident in the figure that, for all systems, $\psi(s = 0,t)$ and $\langle \mathbf{u}(s = 0,t)\cdot\mathbf{u}(s = 0,t = 0)\rangle$ drop to zero practically at the same time, which to a very good approximation is independent of the matrix chain length and composition. The corresponding (characteristic) relaxation time as estimated by fitting the curves with a stretched exponential or KWW (Kohlrausch−Williams−Watts) function of the form $A \exp[-(t/\tau_{KWW})^{\beta_{KWW}}]$ is found to be 3.61 ns for *cis*100-*cis*600 ($\phi_p = 0.375$), 3.13 ns for *cis*200-*cis*600 ($\phi_p = 0.429$), 3.52 ns for *cis*320-*cis*600 ($\phi_p = 0.385$), and 3.75 ns for *cis*1000-*cis*600 ($\phi_p = 0.130$). These values are consistent with the simulation results for the pure *cis*-1,4-PB melts and with a value for the characteristic entanglement time equal to $\tau_e = 2.3\pm0.8$ ns (based on an analysis of the atomistic msd).[39,55]

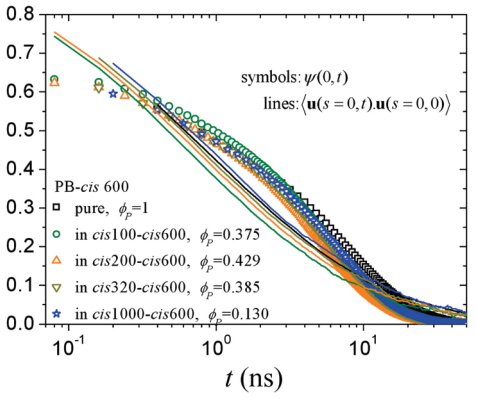

Figure 5. End-segment relaxation of C_{600} probe chains in different matrices based on $\psi(s = 0,t)$ (symbols) or on the time autocorrelation function $\langle \mathbf{u}(s = 0,t)\cdot\mathbf{u}(s = 0,0)$ of the tangent unit vector $\mathbf{u}$ for end segments (lines).

In Figure 6 we analyze the effect of matrix composition on the function $\psi(s,t)$ at constant matrix chain length. We have considered two matrix chain lengths, C_{200} and C_{320}, and we have varied the concentration of the probe chains to examine how this affects their relaxation dynamics. The results are presented at the same time instances as those in Figure 4, except for the data at $t = 2$ ns which we did not include since at this very early time, as we saw in Figure 4, the $\psi(s,t)$ curves are practically the same in all of the simulated systems. At $t = 7.5$ ns (still an early time), matrix composition seems not to play a significant role for the dynamics of the probe chains (although one can notice that, as the volume fraction ϕ_p of the C_{600} probe chain decreases, the values of $\psi(s,t)$ become slightly smaller), indicating that the CR mechanism is not yet present. At later times, e.g., for $t = 32$ ns and $t = 106$ ns, compositional effects on the dynamics of the probe chains become more obvious: Figure 6b,c shows that as ϕ_p decreases, the rate with which the corresponding functions $\psi(s,t)$ decay to zero is substantially enhanced.

Let us look now into the overall tube survival probability $\Psi(t) = \int_0^1 \psi(s,t)\,ds$ of the C_{600} probe chains and its time decay with respect to matrix chain length and matrix volume fraction in probe chains ϕ_p. According to the plots shown in Figure 7a, the $\Psi(t)$ curves in the pure component PB-*cis*600 melt and in the C_{1000} *cis*-1,4-PB matrix are practically indistinguishable from each other (except at the very late times where a very slight deviation is discernible). This feature should be attributed to the absence of any additional CR effects on the relaxation of the C_{600} *cis*-1,4-PB chains (except those arising from their own relaxation) due to the slower relaxation of the significantly longer C_{1000} *cis*-1,4-PB matrix chains. In sharp contrast, the rate of decay of the function $\Psi(t)$ in the three shorter chain matrices (*cis*100-*cis*600, *cis*200-*cis*600, and *cis*320-*cis*600) is considerably faster than in the pure component PB-*cis*600 melt, an indication of non-negligible CR effects associated with the (fast) relaxation of the short matrix chains. Clearly, the matrix chain length plays a key role in the relaxation of the tagged chains to the degree that we can claim that it practically controls their overall relaxation dynamics. How

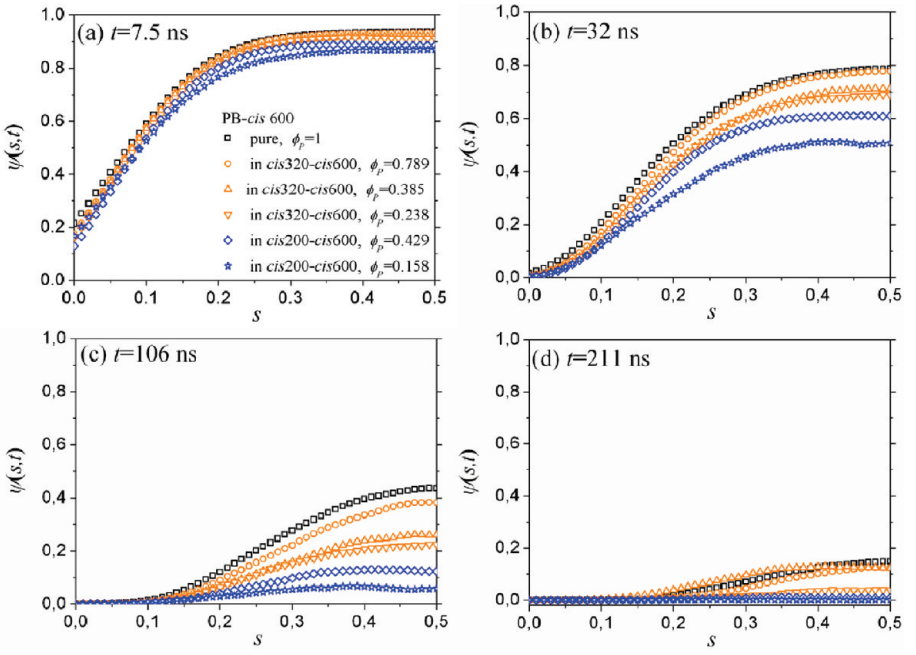

Figure 6. Effect of the volume fraction ϕ_p of the C_{600} *cis*-1,4-PB probe chains on their segment survival probability function $\psi(s,t)$ in the *cis*200-*cis*600 and *cis*320-*cis*600 binary mixtures. Profiles of computed $\psi(s,t)$ curves at (a) $t = 7.5$ ns ($\sim 3\tau_e$), (b) $t = 32$ ns ($\sim \tau_R/3$), (c) $t = 106$ ns ($\sim \tau_R$), and (d) $t = 211$ ns ($\sim \tau_d/2$).

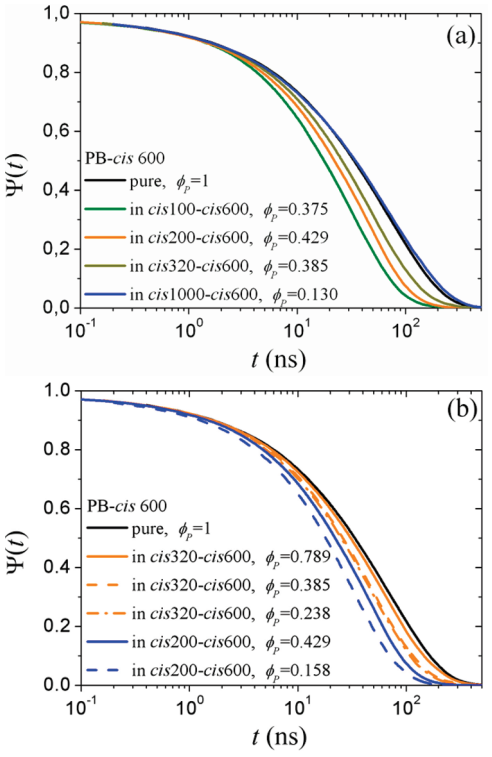

Figure 7. Overall tube survival probability $\Psi(t) = \int_0^1 \psi(s,t)\,ds$ for C_{600} *cis*-1,4-PB probe chains in different matrices and its variation with respect to (a) matrix chain length and (b) matrix composition (volume fraction ϕ_p of probe chains).

the matrix concentration in probe chains affects their dynamics while keeping the matrix chain length constant is shown in Figure 7b. The observation is that $\Psi(t)$ assumes larger values as ϕ_p increases. This is reasonable since topological constraints on a probe chain by other C_{600} probe chains become less and less as ϕ_p decreases in a matrix composed of shorter chains than the probe molecules. It is a conclusion fully consistent with the one we drew from Figure 6 on the basis of the computed $\psi(s,t)$ graphs and in very good agreement with direct experimental measurements.[22,26−31]

Of big interest here is to examine the degree to which terminal relaxation in the simulated bidisperse melts can be categorized in the four different regions as proposed by Viovy et al.[33] depending on the values of $\alpha \equiv M_S^3/M_L M_e^2 = r_{SG}^{-1}$ and $\beta \equiv (M_L/M_e)\phi_L$: (i) tube Rouse ($\alpha < 1$ and $\beta < 1$), (ii) chain reptation I [($\alpha > 1$ and $\beta < 1$) or ($\beta > 1$ and $\alpha > \beta^2$)], (iii) chain reptation II ($\beta > 1$ and $1/\beta < \alpha < \beta^2$), and (iv) tube reptation ($\beta > 1$ and $\alpha\beta < 1$). The values of the parameters α and β that correspond to the bidisperse melts simulated in this work are reported in Table 1; on the basis of them, we can then try to examine if each one of them follows the specific classification proposed by Viovy et al.[33] However, we have to be very cautious in such an effort because the exact quantitative values of the parameters α and β separating the different regimes are not precisely known due to the large number of assumptions behind the theory. For instance, the crossover value for α from experimental data is quite broad ranging from 2 to 10.[18,29,56] Furthermore, while the Viovy et al.[33] theory is well suited for bidisperse melts comprising sufficiently long chains for both the long and the short components (except the extreme case of $M_S < M_e$), our simulated bidisperse melts are only moderately entangled, rendering their classification even more difficult. Given all these difficulties and uncertainties, it seems more logical to examine the degree to which our simulated systems follow the Viovy et al.[33] classification by checking how the characteristic relaxation time τ_c for each system based on the

Table 1. Values of the Parameters α and β Determining the Various Dynamical Regimes in the Viovy et al. Theory (see Figure 6 in Ref 33) and Simulation Results for the Characteristic Relaxation Time τ_c of the Simulated Systems[a]

system	ϕ_L	α^b	β^c	$\alpha\beta$	τ_c (ns)
*cis*100-*cis*600	0.375	0.080	1.563	0.126	29.5
*cis*100-*cis*600	0.545	0.080	2.273	0.183	36.6
*cis*200-*cis*600	0.158	0.643	0.658	0.423	29.2
*cis*200-*cis*600	0.429	0.643	1.786	1.148	36.7
*cis*320-*cis*600	0.238	2.634	0.992	2.613	44.3
*cis*320-*cis*600	0.385	2.634	1.603	4.221	46.3
*cis*320-*cis*600	0.789	2.634	3.289	8.664	57.9

[a] As explained in the text, τ_c has been estimated by the integral of the stretched-exponential curve ($A\ \exp[-(t/\tau_{KWW})^{\beta_{KWW}}]$) describing the decay of the overall survival probability function $\Psi(t)$; for the pure component PB-*cis*600 melt, its value is approximately equal to 65 ns (ref 55). [b] α is defined as $M_S^3/M_L M_e^2$; therefore, it is equal to r_{SG}^{-1}. [c] β is defined as $(M_L/M_e)\phi_L$.

relaxation of the overall survival probability function $\Psi(t)$ varies from matrix to matrix, i.e., as a function of the values of α and β. To follow such an approach, we first computed the value of τ_c for each system by integrating the stretched-exponential curve ($A\ \exp[-(t/\tau_{KWW})^{\beta_{KWW}}]$) describing the decay of the corresponding overall survival probability function $\Psi(t)$; the results are shown in the last column of Table 1. Then on the basis of the variation of τ_c with the volume fraction ϕ_p (= ϕ_L for the systems of Table 1) of the probe chains and by taking into consideration the computed values for the parameters α, β, and $\alpha\beta$ for the simulated systems, we conclude the following: (a) The *cis*100-*cis*600 and *cis*200-*cis*600 binary mixtures should be near the border of the tube Rouse and tube reptation regimes; furthermore, the stronger dependence of τ_c on ϕ_p for the *cis*100-*cis*600 system is considered as being more characteristic of the tube reptation regime. (b) The *cis*320-*cis*600 system should lie in the regime of chain reptation I for $\phi_p = 0.238$ and $\phi_p = 0.385$ and in the region of chain reptation II for $\phi_p = 0.789$. But the reader should always remember that all these estimates are very approximate since they refer to bidisperse systems that are only weakly entangled.

How the presence of a few longer chains affects the relaxation of shorter matrix chains (for example, how the presence of the longer C_{600} probe chains in our simulations affects the dynamics of matrix chains with length equal to C_{320} and C_{200}) is further analyzed in Figure 8. The figure shows simulation results for the function $\psi(s,t)$ referring to the C_{320} *cis*-PB matrix chains in various *cis*320-*cis*600 binary mixtures, i.e., for different values of the volume fraction ϕ_p of the longer chains. As expected, at very early times comparable to the characteristic entanglement time τ_e of the C_{320} *cis*-PB chains (e.g., for $t = 1.4$ ns), the obtained $\psi(s,t)$ curves are practically the same and, within the statistical uncertainty, identical to those in their own melt (the PB-*cis*320 melt in Figure 8a). As time increases, however, systematic deviations are observed (Figure 8b,c) between the various binary mixtures and the pure component system (PB-*cis*320 melt). In this respect, our simulation results provide molecular-level support for the proposed approaches of CR in entangled polymers known today as dynamic dilution,[14,18,56,57] double reptation,[13,16] and self-consistent CR.[15] Also, once more, we notice that any differences in the $\psi(s,t)$ curves between different systems diminish for segments near chain ends, $s \le 0.15$ or, equivalently, $s \ge 0.85$. One is led to the same conclusion by analyzing the corresponding simulation findings for the overall relaxation function $\Psi(t)$ for the matrix chains, which are reported in Figure 9: increasing the concentration of the few longer C_{600} probe chains slows down the relaxation of the shorter matrix chains. As far as the origin of the relatively smaller differences in the results reported in Figure 9 among the various systems (compared to, e.g., those reported in Figure 7) is concerned, this should be sought to the overly large

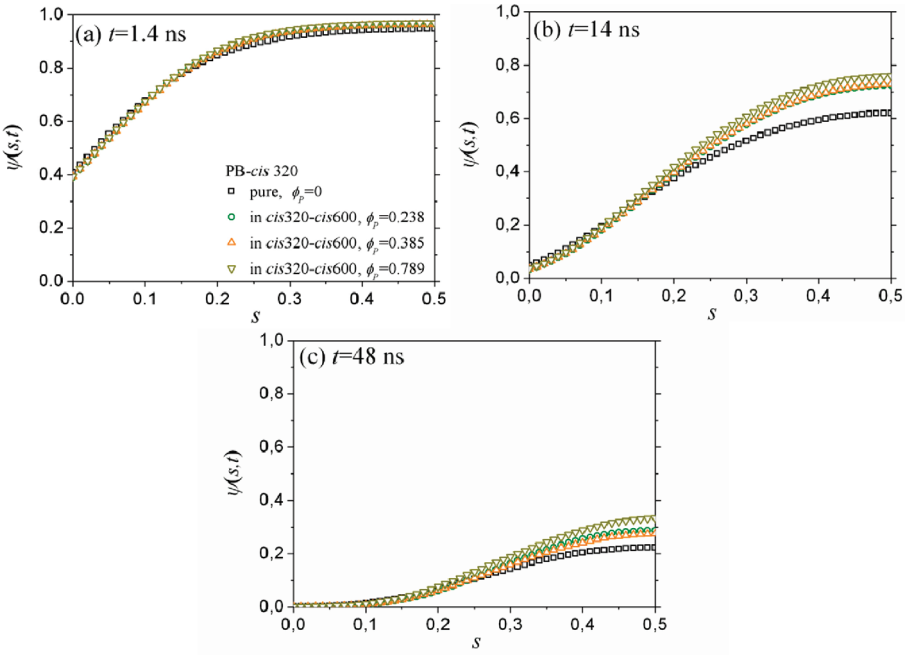

Figure 8. Plots of the segment survival probability function $\psi(s,t)$ for the matrix chains (C_{320} *cis*-1,4-PB) at different volume fractions of the longer chains (C_{600} *cis*-1,4-PB). Simulation results at several times: (a) t = 1.4 ns ($\sim\tau_e$), (b) t = 14 ns ($\sim\tau_R/2$), and (c) t = 48 ns ($\sim\tau_d/3$). τ_e, τ_d, and τ_R here denote the characteristic entanglement, disentanglement, and Rouse times, respectively, of the C_{320} *cis*-1,4-PB chains in their own melt at T = 413 K and P = 1 atm. Their numerical values are[42] $\tau_e = 1.8 \pm 0.4$ ns, $\tau_d = 138 \pm 18$ ns, and $\tau_R = 22 \pm 5$ ns.

contribution of the CLF mechanism to the relaxation of such weakly entangled systems as the C_{320} *cis*-PB melts studied here.

From a statistical mechanics point of view, the relaxation modulus $G(t)$ can also be calculated via the stress−stress autocorrelation function of the off-diagonal elements of the instantaneous stress tensor $\boldsymbol{\sigma}(t)$ (the Green−Kubo formula):[58−62]

$$G(t) = \frac{V}{k_B T}\langle \sigma_{\alpha\beta}(t)\sigma_{\alpha\beta}(0)\rangle, \quad \alpha \neq \beta = x, y, z \qquad (1)$$

where V denotes the system volume, T the temperature, and k_B the Boltzmann constant. Because of the strong fluctuations in the value of the instantaneous atomistic stress tensor $\boldsymbol{\sigma}(t)$,[39] a direct application of eq 1 in fully atomistic models of polymers has been realized so far only for rather short polymer molecules and for very short times (e.g., $t \leq 10$ ps).[60−62] Hindered by this, we have carried out here the Green−Kubo calculation by approximating the stress tensor $\boldsymbol{\sigma}(t)$ through the following expression:[39]

$$\sigma_{\alpha\beta} = \frac{1}{V}\sum_{i=1}^{N_{chain}}\sum_{a=1}^{Z_i} r_{ia,\alpha}F_{ia,\beta}$$

$$= \frac{3k_B T}{V\langle R^2\rangle}\sum_{i=1}^{N_{chain}} L_i \sum_{a=1}^{Z_i} r_{ia,\alpha}u_{ia,\beta}, \quad \alpha \neq \beta = x, y, z \qquad (2)$$

relying on the entropic tensile force of rubber elasticity theory, namely that $\mathbf{F}_{ia} = (3k_B T/\langle R^2\rangle)L_i\mathbf{u}_{ia}$, where $\mathbf{u}_{ia}$, Z_i, and L_i denote the unit vector of the ath entanglement strand, the number of entanglement strands, and the PP contour length of chain i, respectively. The corresponding results for the various bidisperse mixtures are reported in Figure 10 where they are further compared to the results obtained from the direct PP analysis (based on the computed $\Psi(t)$ functions in Figure 7) and the autocorrelation function $\langle \mathbf{R}(t)\cdot\mathbf{R}(0)\rangle/\langle R^2\rangle$ of the chain end-to-end vector $\mathbf{R}$. It is seen that the function $\langle \mathbf{R}(t)\cdot\mathbf{R}(0)\rangle/\langle R^2\rangle$ exhibits overall a slower relaxation behavior compared to those of $\Psi(t)$ from the direct PP analysis and of stress tensor from the Green−Kubo calculation; this is ascribed to the inability of $\langle \mathbf{R}(t)\cdot\mathbf{R}(0)\rangle/\langle R^2\rangle$ to account for local CR effects (similar behaviors have been reported for pure PB melts[39]). In spite, however, of the very approximate formula for the stress tensor, the Green−Kubo prediction appears to be in reasonable agreement with $\Psi(t)$ for all bidisperse systems, especially at late times. The deviation at early to-intermediate time scales is mainly attributed to the purely entropic origin of the stress formula (eq 2); it is also associated with the neglect of local contributions at length scales shorter than the tube diameter or the PP step length.

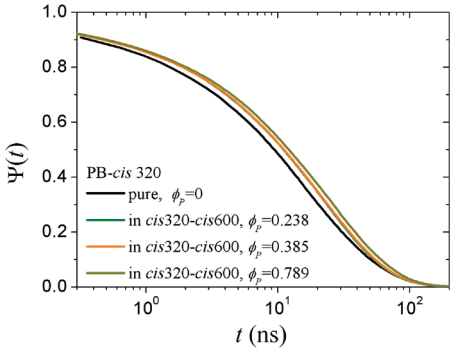

Figure 9. Plots of the overall tube survival probability function $\Psi(t)$ for the C_{320} *cis*-1,4-PB matrix chains at different volume fractions of the C_{600} *cis*-1,4-PB probe chains.

In the framework of the tube model, additional information about the relaxation dynamics in entangled polymers is provided by the time decay of the autocorrelation function $(\langle L(t)L(0)\rangle - \langle L\rangle^2)/(\langle L^2\rangle - \langle L\rangle^2)$ of the PP contour length L. The results obtained for the systems simulated here are shown in Figure 11. More precisely, in Figure 11a we show the computed $(\langle L(t)L(0)\rangle - \langle L\rangle^2)/(\langle L^2\rangle - \langle L\rangle^2)$ vs t curves for the relaxation of the tagged C_{600} *cis*-1,4-PB chains as a function of matrix chain length and in Figure 11b as a function of matrix concentration in probe chains. Figure 11a reveals a strong dependence of the computed $(\langle L(t)L(0)\rangle - \langle L\rangle^2)/(\langle L^2\rangle - \langle L\rangle^2)$ curves on matrix chain length, a result which at first sight contradicts the data

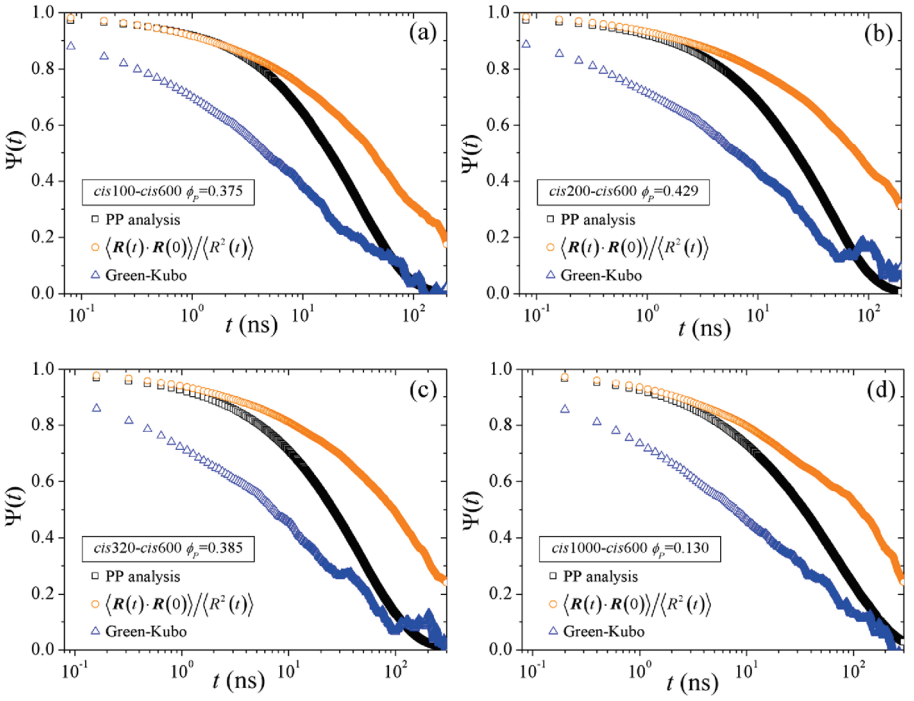

Figure 10. Comparison of the relaxation curves for the C_{600} *cis*-1,4-PB probe chains as obtained from the three different methods discussed in the main text: (i) the direct PP analysis, (ii) the coarse-grained Green−Kubo calculation (eqs 1 and 2), and (iii) the time autocorrelation function $\langle \mathbf{R}(t)\cdot\mathbf{R}(0)\rangle/\langle R^2\rangle$ of the chain end-to-end vector **R**. The results refer to (a) the *cis*100-*cis*600 ($\phi_p = 0.375$), (b) the *cis*200-*cis*600 ($\phi_p = 0.429$), (c) the *cis*320-*cis*600 ($\phi_p = 0.385$), and (d) the *cis*1000-*cis*600 ($\phi_p = 0.130$) system.

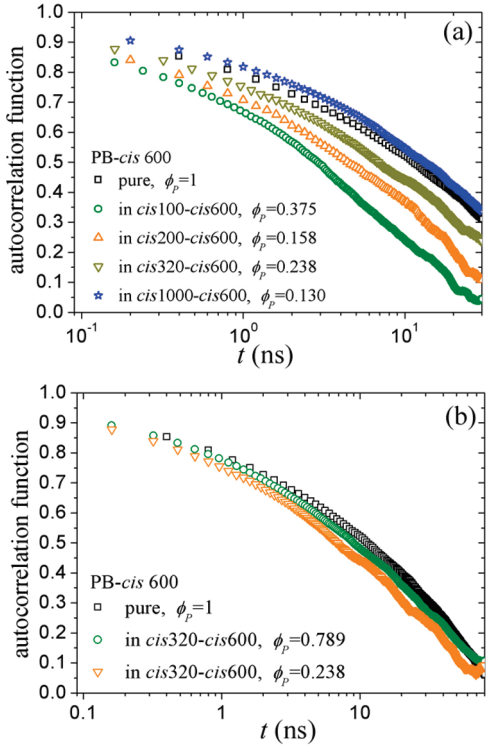

Figure 11. Plots of the time autocorrelation function $(\langle L(t)L(0)\rangle - \langle L\rangle^2)/(\langle L^2\rangle - \langle L\rangle^2)$ for the PP contour length L of the C_{600} *cis*-1,4-PB probe chains in the different matrices with respect to (a) matrix chain length and (b) volume fraction ϕ_p of the C_{600} *cis*-1,4-PB probe chains.

shown in Figures 1 and 2b that the average value of the PP contour length $\langle L\rangle$ and of its fluctuation $\langle L^2\rangle$ are independent of the detailed matrix characteristics. This apparent conflict is resolved if one accepts that static and dynamic properties are affected differently by factors such as the exact molecular length of the matrix chains and the relative concentration of short and long components. Indeed, that the values of $\langle L\rangle$ and $\langle L^2\rangle$ for C_{600} *cis*-1,4-PB chains are the same in the various binary mixtures and in their own melt implies that the average number of entanglements and the corresponding fluctuations are the same among all systems. However, this should not imply that the average rate of entanglement creation or destruction would be the same as well. In fact, the rate with which entanglements are released or redeveloped should get larger as the length of the matrix chains decreases. Thus, the entanglement dynamics of tagged C_{600} chains is faster in binary mixtures with shorter chains. And since the corresponding relaxation time for the $\langle L(t)L(0)\rangle$ function is proportional to the magnitude of this rate, $(\langle L(t)L(0)\rangle - \langle L\rangle^2)/(\langle L^2\rangle - \langle L\rangle^2)$ will decay to zero faster in mixtures where matrix chains have a shorter length than tagged ones. This is exactly what the curves presented in Figure 11a demonstrate. With the same reasoning, if we keep the matrix chain length constant, $(\langle L(t)L(0)\rangle - \langle L\rangle^2)/(\langle L^2\rangle - \langle L\rangle^2)$ is expected to decay more rapidly in the mixtures with a smaller concentration in longer (tagged) chains, which is what we see in the plots of Figure 11b: $(\langle L(t)L(0)\rangle - \langle L\rangle^2)/(\langle L^2\rangle - \langle L\rangle^2)$ drops slower in the systems characterized by a higher ϕ_p value, i.e., in the systems where the dynamics of the entanglement interaction is on the average slower due to the larger percentage of longer C_{600} chains.

In the tube theory, the function $\Psi(t)$ for the overall relaxation of the primitive chain is of paramount importance since its knowledge allows one to compute the spectra of storage $G'(\omega)$ and loss $G''(\omega)$ moduli of the melt through a simple Fourier transform:

$$G'(\omega) = G_N^0 \omega \int_0^\infty \Psi(t)\sin(\omega t)\,dt;$$
$$G''(\omega) = G_N^0 \omega \int_0^\infty \Psi(t)\cos(\omega t)\,dt \quad (3)$$

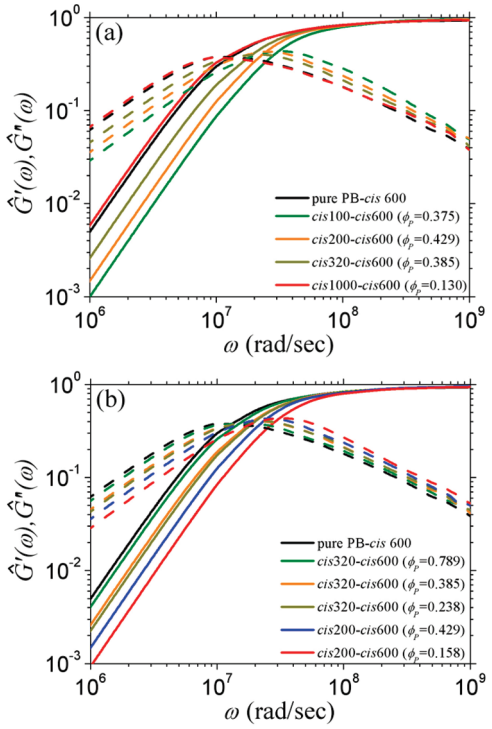

Figure 12. Effect of (a) matrix chain length and (b) matrix composition on the contribution of the C_{600} *cis*-1,4-PB probe chains to the storage $G'(\omega)$ (solid lines) and loss $G''(\omega)$ (dashed lines) moduli of the system (results normalized with the plateau modulus G_N^0; $\hat{G}'(\omega) \equiv G'(\omega)/G_N^0$ and $\hat{G}''(\omega) \equiv G''(\omega)/G_N^0$).

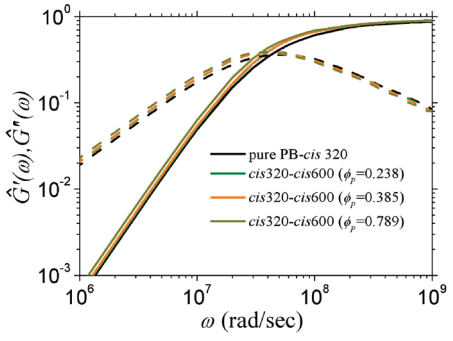

Figure 13. Effect of the volume fraction ϕ_p of C_{600} *cis*-1,4-PB probe chains on the matrix chain contribution to the storage $G'(\omega)$ (solid lines) and loss $G''(\omega)$ (dashed lines) moduli of the *cis*320-*cis*600 melts.

where G_N^0 is the plateau modulus. For a binary polymer mixture, in particular, where one can distinguish between two different $\Psi(t)$ functions (one for the short species and one for the long species), one can also speak of two different contributions to these spectra: one from the short chains and one from the long chains. Thus, in the following, three sets of curves are reported: the first set (Figure 12) refers to the contribution to the $G'(\omega)$ and $G''(\omega)$ spectra (normalized by G_N^0) from the reptation dynamics *of the probe chains only*; the second set (Figure 13) provides the contribution to the $G'(\omega)$ and $G''(\omega)$ spectra from the long-time relaxation of *short matrix chains only* in each system; and the third set (Figure 14) refers to the *total* (*both short and long species*) $G'(\omega)$ and $G''(\omega)$ spectra for each system obtained by including also the contributions of the Rouse modes capturing dynamics at times shorter than reptation (and its accompanying or competing mechanisms: CR and CLF).

Focusing first on the set of curves shown in Figure 12, we see that as the matrix chain length decreases, the part of the $G'(\omega)$ and

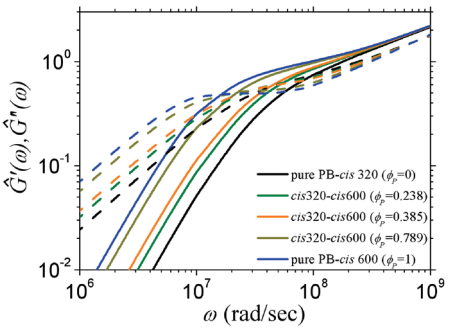

Figure 14. Computed spectra of storage $G'(\omega)$ and loss $G''(\omega)$ moduli in the *cis*320-*cis*600 melts. Rouse mode contributions have been accounted according to Milner and McLeish[57] (see text).

$G''(\omega)$ spectra connected with the reptation of the probe C_{600} chains shifts to higher frequencies ω, which indicates smaller values for the characteristic relaxation times of the tagged C_{600} chains in matrices with shorter chain lengths compared to their own melt (the PB-*cis*600 melt). We also notice in the figure that the widening of the characteristic time scales is not uniform in the low- and high-frequency regimes. More precisely, the decrease of the time scales is more uniform in the low-frequency regime than it is in the high-frequency regime (e.g., for $\omega \geq \omega_{max}$ where ω_{max} is the frequency at which $G''(\omega)$ attains its maximum), indicating that C_{600} probe chains are predominantly affected by matrix chain length on longer time scales. This result is consistent with the conclusions drawn from the analysis of the simulation data reported in Figure 7a. In Figure 12b we present the corresponding results with respect to matrix concentration in long (tagged) and short chains: for each binary system (*cis*200-*cis*600 or *cis*320-*cis*600), the set of the $G'(\omega)$ and $G''(\omega)$ curves shifts to higher frequencies as the volume fraction ϕ_p of the longer chains decreases, which again agrees with the conclusions drawn from the analysis of the simulation results for $\Psi(t)$ shown in Figure 7b. The same conclusions are reached by analyzing the data shown in Figure 13 for the contributions to the functions $G'(\omega)$ and $G''(\omega)$ of the C_{320} *cis*-1,4-PB chains in the C_{320} matrix at different concentrations of the C_{600} probe chains. Because of the dominance of CR effects associated with the fast relaxation of the relatively short chains making up the matrix (cf. Figure 9), the contribution to $G'(\omega)$ and $G''(\omega)$ from the relaxation of the probe chains causes a shift of the spectra to lower frequencies as ϕ_p increases.

Lastly, in Figure 14 we compare the total storage $G'(\omega)$ and loss $G''(\omega)$ moduli in the different binary mixtures, i.e., by also taking into account Rouse mode contributions. To this end, we have added to the $G(t)$ curves obtained from the Fourier transform of the total $\Psi(t)$ function (the one referring to the weighted sum of the corresponding functions for short and long chain species in the system) the following contribution:

$$\frac{G_N^0}{Z_{app}}\left[\frac{1}{3}\sum_{i=1}^{Z_{app}}\exp\left(-\frac{2p^2t}{\tau_R}\right)+\sum_{i=Z_{app}+1}^{N}\exp\left(-\frac{2p^2t}{\tau_R}\right)\right] \quad (4)$$

In eq 4, Z_{app} denotes the number of apparent entanglement segments calculated as M/M_e (distinguished from the number of physical entanglement strands Z directly obtained from topological analysis by Z1 as reported in Figure 2a) and N the number of atoms per chain. The first term represents the contribution of the longitudinal Rouse motion along the one-dimensional curvilinear tube and the second the contribution of the three-dimensional Rouse motion. This treatment was first suggested by Milner and McLeish[57] and has been adopted by many other researchers in the field afterward.[51,63,64] Figure 14 shows the

dynamic moduli for all different composition *cis*320-*cis*600 binary mixtures simulated in this work, ranging from the pure component PB-*cis*320 melt to the pure component PB-*cis*600 melt. As the concentration of the C_{600} probe chain is increased in a C_{320} *cis*-1,4-PB matrix, the computed $G'(\omega)$ and $G''(\omega)$ spectra are extended to lower frequencies, indicating the emergence of longer characteristic time scales than those corresponding to the pure component PB-*cis*320 melt. We further notice that the $G''(\omega)$ spectra of our simulated systems show only one peak as compared to two peaks observed quite often in experimental samples under certain conditions,[29,31] corresponding to the loss peaks for the short and long chain components; this should be attributed to the relatively low molecular weight of the simulated systems and to the rather narrow gap in the molecular weights between short and long components.

4. Conclusions and Outlook

We have analyzed the viscoelastic properties of model bidisperse *cis*-1,4-PB melts in terms of the segment survival probability $\psi(s,t)$ and of the overall probability $\Psi(t)$ for short and long chains as a function of matrix chain length and composition. Bidisperse polymers are ideal systems for capturing CR effects on chain dynamics at the most fundamental level because of the flexibility they offer to control rather precisely the lifetime of entanglements on test chains by tuning the molecular properties (chain length and composition) of the matrix. The results have been obtained by employing a recently developed computational methodology[39] that allows one to reduce atomistic trajectories accumulated in the course of long MD simulations to trajectories of primitive paths and then make the connection with the tube model by studying primitive segment motion through the space of an effective curvilinear tube around the main chain contour. We have found that the relaxation of the test chains is accelerated if we reduce the matrix chain length or the concentration of the longer component in the system, which reveals the dominant role of CR in the viscoelastic properties of these systems. On the other hand, while the magnitude of CLFs of the probe chains has been found to be practically insensitive to the molecular details of the matrix (chain length and composition), CR has been seen to affect considerably the rate with which the time autocorrelation function of the PP contour length decays to zero. The decay is accelerated when the length of the matrix chains or the concentration of the longer chains in the matrix decreases. We have also studied the inverse effect, namely, how the profiles of the $\psi(s,t)$ and $\Psi(t)$ functions of the matrix chains are affected by the presence of longer probe chains, especially at higher concentration of the latter. The corresponding findings underline the importance of CR effects even for monodisperse systems, especially when these are composed of weakly entangled chains.

In a second step, the computed $\psi(s,t)$ and $\Psi(t)$ profiles for short and long chains in the simulated binary polymer melts have been used to compute the storage $G'(\omega)$ and loss $G''(\omega)$ moduli. This allowed us to study CR effects also at the level of the linear viscoelastic properties of the simulated systems.

The conclusions drawn from our work are consistent with available experimental data;[22,26−31] they also support theoretical arguments proposed to account for the extra relaxational mechanisms present in polydisperse polymer systems.[32,33] For example, our simulations suggest that *tube dilation* in binary mixtures is important, and thus of relevance, only when the molecular weight of the shorter chains is less than the characteristic entanglement molecular weight M_e. More precisely, for the C_{600} *cis*-1,4-PB chains addressed here, we mention that the tube diameter was computed to be equal to ∼30 Å in all binary mixtures with $M_S > M_e$ (also the value in their own melt), but this was increased to ∼32−40 Å in the matrix composed of chains shorter than C_{144} *cis*-1,4-PB molecules at $\phi_p = 0.375-0.545$. This is a significantly result of our analysis directly corroborating the hypothesis of Viovy et al.[33]

Our simulation data for $G(t)$ or $G'(\omega)$ and $G''(\omega)$ can be directly compared against experimental data measured on actual *cis*-1,4-PB bidisperse melts. Unfortunately, the MW of the probe chains employed in experiment measurements of 1,4-PB melts[26,30,31] are significantly higher (by about 6−50 times) than the C_{600} probe chains employed in this study. On the other hand, our simulated systems are pure *cis*-1,4-PB bidisperse melts whereas the experimental samples are in their majority mixtures of *cis*-1,4-PB and *trans*-1,4-PB containing also a small amount (about 5−10%) of the 1,2-PB component. These issues render the direct comparison between simulated and measured viscoelastic properties for *cis*-1,4-PB melts of limited or questionable value. But with recent advances in the field, which have made it possible to synthesize pure *cis*-1,4-PB melts of relatively low molecular weight,[65] such a direct comparison may not be too far away to materialize.

Closely related to the issue of CR addressed here in the different matrices is that of the lifetime of entanglements. Considering topological constraints as binary contacts, such an analysis would help analyze the relationship between CR effects and average time for the creation/destruction of entanglement points separately from short and long chains. Unfortunately, with the Z1-code employed in our study, such an analysis is not possible at the moment: (a) the precise location of entanglements along the chain is uncertain, (b) not all geometric kinks correspond to true entanglements, and (c) there is always the possibility in the code for kinks that involve more than two chains. Given that these aspects are not specific to Z1 but also to the two other methodologies developed so far for reducing atomistic trajectories to primitive paths (PPA[66] and CReTA[47]), resolving them would be highly desirable not only for a better understanding of the CR mechanism itself in bidipserse (and polydisperse) polymer samples but also for separating the dynamic tube dilation (DTD) mechanism from the CR-Rouse one in such systems.[56]

Our work can be extended rather straightforwardly to flowing polymer melts in an effort to rationalize how the computed $\psi(s,t)$ and $\Psi(t)$ profiles are affected by the applied flow field. This could help capture not only thermal but also convective CR (CCR)[67] effects on chain dynamics which are supposed to play an important role in nonequilibrium systems. The presented approach has the potential to reveal the microscopic origin of the CCR mechanism, thereby guiding theoreticians in their efforts to develop tube models with an even higher predictive capability of polymer melt rheology.

Acknowledgment. We feel deeply indebted to Dr. Evelyne van Ruymbeke for her personal interest in this work and her help with the design of the MD simulation runs for many of the bidisperse systems addressed here. Support provided by the European Commission through the MODIFY (FP7-NMP-2008-SMALL-2, Code 228320) research project is greatly acknowledged. G.T. also acknowledges the support of the State Scholarships Foundation of Greece. M.K. acknowledges support by the Swiss National Science Foundation through Grant IZ73Z0-128169.

References and Notes

(1) Ferry, J. D. *Viscoelastic Properties of Polymers*, 3rd ed.; John Wiley & Sons: New York, 1980.
(2) Bird, R. B.; Curtiss, C. F.; Armstrong, R. C.; Hassager, O. *Dynamics of Polymeric Liquids, Fluid Mechanics*, 2nd ed.; John Wiley & Sons: New York, 1987; Vols. *1* and *2*.
(3) Doi, M.; Edwards, S. F. *The Theory of Polymer Dynamics*; Clarendon Press: New York, 1986.

(4) Edwards, S. F. *Proc. Phys. Soc.* **1967**, *92*, 9.
(5) Edwards, S. F. *Polymer* **1977**, *9*, 140.
(6) de Gennes, P. G. *J. Chem. Phys.* **1971**, *55*, 572.
(7) (a) Doi, M.; Edwards, S. F. *J. Chem. Soc., Faraday Trans. 2* **1978**, *74*, 1789. (b) *Ibid.* **1978**, *74*, 1802. (c) *Ibid.* **1978**, *74*, 1818.
(8) (a) Doi, M. *J. Polym. Sci., Polym. Lett. Ed.* **1981**, *19*, 265. (b) *J. Polym. Sci., Polym. Phys. Ed.* **1983**, *21*, 667.
(9) de Gennes, P. G. *Macromolecules* **1976**, *9*, 587.
(10) de Gennes, P. G. *Scaling Concepts in Polymer Physics*; Cornell University Press: Ithaca, NY, 1979.
(11) Klein, J. *Macromolecules* **1978**, *11*, 852.
(12) Graessley, W. W. *Adv. Polym. Sci.* **1982**, *47*, 67.
(13) Viovy, J. L. *J. Phys.* (*Paris*) **1985**, *46*, 847.
(14) Marrucci, G. *J. Polym. Sci., Polym. Phys. Ed.* **1985**, *23*, 159.
(15) Rubinstein, M.; Colby, R. H. *J. Chem. Phys.* **1988**, *89*, 5291.
(16) des Cloizeaux, J. *Europhys. Lett.* **1988**, *5*, 437.
(17) Ball, R. C.; McLeish, T. C. B. *Macromolecules* **1989**, *22*, 1911.
(18) Watanabe, H. *Prog. Polym. Sci.* **1999**, *24*, 1253.
(19) McLeish, T. C. B. *Adv. Phys.* **2002**, *51*, 1379.
(20) (a) Green, P. F.; Mills, P. J.; Palmstrom, C. J.; Mayer, J. W.; Kramer, E. J. *Phys. Rev. Lett.* **1984**, *53*, 2145. (b) Green, P. F.; Kramer, E. J. *Macromolecules* **1986**, *19*, 1108.
(21) Antonietti, M.; Coutandin, J.; Sillescu, H. *Macromolecules* **1986**, *19*, 793.
(22) Watanabe, H.; Kotaka, T. *Macromolecules* **1987**, *20*, 530.
(23) Tead, S. F.; Kramer, E. J. *Macromolecules* **1988**, *21*, 1513.
(24) Von Seggern, J.; Klotz, S.; Cantow, H.-J. *Macromolecules* **1991**, *24*, 3300.
(25) Rathgeber, S.; Willner, L.; Richter, D.; Brulet, A.; Farago, B.; Appel, M.; Fleischer, G. *J. Chem. Phys.* **1999**, *110*, 10171.
(26) Wang, S.; von Meerwall, E. D.; Wang, S.-Q.; Halasa, A.; Hsu, W.-L.; Zhou, J. P.; Quirk, R. P. *Macromolecules* **2004**, *37*, 1641.
(27) Masuda, T.; Kitagawa, K.; Inoue, T.; Onogi, S. *Macromolecules* **1970**, *3*, 116.
(28) Watanabe, H.; Kotaka, T. *Macromolecules* **1984**, *17*, 2316.
(29) Struglinski, M. J.; Graessley, W. W. *Macromolecules* **1985**, *18*, 2630.
(30) Juliani; Archer, L. A. *J. Rheol.* **2001**, *45*, 691.
(31) Wang, S.; Wang, S.-Q.; Halasa, A.; Hsu, W.-L. *Macromolecules* **2003**, *36*, 5355.
(32) Doi, M.; Graessley, W. W.; Helfand, E.; Pearson, D. S. *Macromolecules* **1987**, *20*, 1900.
(33) Viovy, J. L.; Rubinstein, M.; Colby, R. H. *Macromolecules* **1991**, *24*, 3587.
(34) Baschnagel, J.; Paul, W.; Tries, V.; Binder, K. *Macromolecules* **1998**, *31*, 3856.
(35) Lin, H.; Mattice, W. L.; von Meerwall, E. D. *Macromolecules* **2007**, *40*, 959.
(36) Barsky, S. *J. Chem. Phys.* **2000**, *112*, 3450.
(37) Picu, R. C.; Rakshit, A. *J. Chem. Phys.* **2007**, *127*, 144909.
(38) Tsolou, G.; Mavrantzas, V. G., unpublished data.
(39) Stephanou, P. S.; Baig, C.; Tsolou, G.; Mavrantzas, V. G.; Kröger, M. *J. Chem. Phys.* **2010**, *132*, 124904.
(40) Gee, R. H.; Boyd, R. H. *J. Chem. Phys.* **1994**, *101*, 8028.
(41) Smith, G. D.; Paul, W. *J. Phys. Chem. A* **1998**, *102*, 1200.
(42) Tsolou, G.; Mavrantzas, V. G.; Theodorou, D. N. *Macromolecules* **2005**, *38*, 1478.
(43) Plimpton, S. J. *J. Comput. Phys.* **1995**, *117*, 1.
(44) Tuckerman, M.; Berne, B. J.; Martyna, G. J. *J. Chem. Phys.* **1992**, *97*, 1990.
(45) (a) Kröger, M. *Comput. Phys. Commun.* **2005**, *168*, 209. (b) Foteinopoulou, K. N.; Karayiannis, C.; Mavrantzas, V. G.; Kröger, M. *Macromolecules* **2006**, *39*, 4207. (c) Karayiannis, N. C.; Kröger, M. *Int. J. Mol. Sci.* **2009**, *10*, 5054.
(46) Masubuchi, Y.; Ianniruberto, G.; Greco, F.; Marrucci, G. *Int. J. Nano Adv. Eng. Mater., Part A* **2008**, *1*, 35 (also in *Proceedings, AES − ATEMA' 2007 International Conference, Montreal, Canada, Aug 6−10*, **2007**; pp 291−296).
(47) Tzoumanekas, C.; Theodorou, D. N. *Macromolecules* **2006**, *39*, 4592.
(48) Masubuchi, Y.; Ianniruberto, G.; Greco, F.; Marrucci, G. *J. Chem. Phys.* **2003**, *119*, 6925.
(49) Doi, M.; Kuzuu, N. Y. *J. Polym. Sci., Polym. Lett. Ed.* **1980**, *18*, 775.
(50) Milner, S. T.; McLeish, T. C. B. *Macromolecules* **1997**, *30*, 2159.
(51) Pattamaprom, C.; Larson, R. G.; Van Dyke, T. J. *Rheol. Acta* **2000**, *39*, 517.
(52) Kröger, M.; Hess, S. *Physica A* **1993**, *195*, 336.
(53) Aoyagi, T.; Doi, M. *Comput. Theor. Polym. Sci.* **2000**, *10*, 317.
(54) van Ruymbeke, E.; Vlassopoulos, D.; Kapnistos, M.; Liu, C. Y.; Bailly, C. *Macromolecules* **2010**, *43*, 525.
(55) Stephanou, P. S.; Baig, C.; Mavrantzas, V. G. *Soft Matter* **2010**, DOI: 10.1039/C0SM00327A.
(56) Watanabe, H.; Ishida, S.; Matsumiya, Y.; Inoue, T. *Macromolecules* **2004**, *37*, 6619.
(57) Milner, S. T.; McLeish, T. C. B. *Phys. Rev. Lett.* **1998**, *81*, 725.
(58) Sen, S.; Kumar, S. K.; Keblinski, P. *Macromolecules* **2005**, *38*, 650.
(59) (a) Liktmann, A. E.; Sukumaran, S. K.; Ramirez, J. *Macromolecules* **2005**, *40*, 6748. (b) Ramirez, J.; Sukumaran, S. K.; Liktmann, A. E. *J. Chem. Phys.* **2007**, *126*, 244904.
(60) Mondello, M.; Grest, G. S. *J. Chem. Phys.* **1997**, *106*, 9327.
(61) Cui, S. T.; Cummings, P. T.; Cochran, H. D. *J. Chem. Phys.* **1996**, *104*, 255.
(62) Harmandaris, V. A.; Mavrantzas, V. G.; Theodorou, D. N. *Macromolecules* **2000**, *33*, 8062.
(63) van Ruymbeke, E.; Keunings, R.; Stéphenne, V.; Hagenaars, A.; Bailly, C. *Macromolecules* **2002**, *35*, 2689.
(64) Leygue, A.; Bailly, C.; Keunings, R. *J. Non-Newtonian Fluid Mech.* **2006**, *133*, 28.
(65) Kapnistos, M.; van Ruymbeke, E.; Vlassopoulos, D., private communication .
(66) Everaers, R.; Sukumaran, S. K.; Grest, G. S.; Svaneborg, C.; Sivasubramanian, A.; Kremer, K. *Science* **2004**, *303*, 823.
(67) (a) Marrucci, G. *J. Non-Newtonian Fluid Mech.* **1996**, *62*, 279. (b) Ianniruberto, G.; Marrucci, G. *J. Non-Newtonian Fluid Mech.* **1996**, *65*, 241.